Developed Wide-Band Frequency Transformer Model for Conducted Common Mode Characteristics Prediction

Kaining FU, Jiangtao TU, Wei CHEN, and Linsen HUANG

***Abstract*—Isolated power converters are widely used for its safety and flexible adjustment between input and output voltage range. EMI occurs due to the presence of switching process. The existence of parasitic parameters in transformers causes the work of EMI prediction in isolated DC-DC power converters more complicated. Parasitic parameters in transformer are the crucial propagation paths for CM noise conduction. For improving the accuracy of EMI prediction, this paper developed a wide-band frequency transformer model based on the two-capacitance model, further considering both the effect capacitive and inductive coupling on conductive common mode noise. Furthermore, the influence of permeability versus frequency of Mn-Zn ferrite on CM transmission, is investigated in detail. Two-port measurement is used for the validation of the proposed high frequency model. The experiment results demonstrate that the proposed wind-band frequency transformer model can well predict the CM noise behavior in the frequency range of 100 kHz to 100 MHz.**

***Index Terms*—Common mode, electromagnetic interference, high frequency model, parasitic parameter, transformer.**

I. Introduction

ELECTROMAGNETIC interference has become a major challenge in the design of switch-mode power supplies (SMPSs) [1]. Electromagnetic interference (EMI) affects the normal operation of SMPSs, leading to a big size of EMI filters [2]−[3]. The electromagnetic compatibility (EMC) standards are compulsory certification for power converters. For decreasing the volume of EMI filters, various noise suppression methods can be applied [3]−[8].

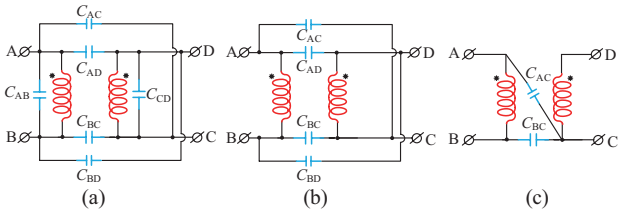

Fig. 1. High-frequency model of transformer. (a) Six-capacitance model, (b) Four-capacitance model, (c) Two-capacitance model.

Isolated DC-DC converters are commonly used in electric vehicle (EV), energy storage systems. The magnetic components have the function of magnetic energy storage, voltage transform and noise filtering. Power converters with transformers show significant advantages in terms of galvanic isolation and larger range of voltage conversion ranges. Therefore, transformers are the key magnetic components in isolated power converters. Parasitic parameters in transformers are key propagation path for CM noise conduction. Various researches are focused on modeling, prediction and suppression of the CM behaviors. M. Antivachis *et al*. [6], H. Chen *et al*. [7]−[8], and Y. Li *et al*. [9] investigated the conduction path of EMI noise in flyback converters and pointed out that reducing capacitive coupling is the key to suppress CM noise. However, the prior art has a limited frequency range when deal with high frequency EMI noise suppression.

The development of accurate transformer model is significant in analyzing, predicting and suppressing EMI noise in SMPSs. Then, several modeling techniques have been developed, only considering the effect of capacitive coupling on CM conduction [10]−[16]. As shown in Fig. 1(a), [11] proposed a six-capacitance model to represent the CM behavior of the transformer. However, [12] points out that not all the capacitances in the model are contribute to CM noise. The capacitors C_{AB} and C_{CD} are connected in parallel with the primary winding and secondary windings and do not generate CM noise. This is because CM noise only flows through the capacitance between the primary and secondary windings. As shown in Fig. 1(b), the six-capacitance model can be simpli-

Manuscript received November 27, 2024; revised January 06, 2025; accepted January 27, 2025. Date of publication March 30, 2025; date of current version February 28, 2025. This work was supported in part by National Natural Science Foundation of China under the grant 51777036, Natural Science Foundation of Xiamen, China under the grant 3502Z202372043, Research start-up fund of Xiamen University of Technology under the grant YKJ23011R, and Innovation Project of Xiamen University of Technology under the grant YKJCX2024162. *(Corresponding author: Kaining Fu.)*

K. Fu and L. Huang are with the Xiamen Key Laboratory of Frontier Electric Power Equipment and Intelligent Control, the School of Electrical Engineering and Automation, Xiamen University of Technology, Xiamen 361024, China (e-mail: fkn@xmut.edu.cn; hls@xmut.edu.cn).

J. Tu is with School of Electrical Engineering and Automation, Xiamen University of Technology, Xiamen 361024, China (e-mail: 1092111621@qq.com).

W. Chen is with School of Electrical Engineering and Automation, Fuzhou University, Fuzhou 350108, China (e-mail: Chw@fzu.edu.cn).

Digital Object Identifier 10.24295/CPSSTPEA.2025.00004

fied as four-capacitance model. [12] pointed out that the capacitance between primary and secondary winding should observe the displacement rule. The number of capacitances can be further reduced. Based on the displacement current law, the four-capacitance model can be simplified to two-capacitance model as shown in Fig. 1(c). Then, H. Zhang *et al*. [12] developed a two-capacitance transformer model and a practical evaluation method for CM behaviors. For further accelerating the optimization process, both [13] and [14] proposed using FEM simulation tools to achieve the optimization of transformer. EMI suppression of transformers can be addressed at the designed stage. However, all of the above techniques are focused on reducing the capacitive coupling of the transformer to achieve noise suppression.

With further investigation on high-frequency modeling, more attenuation should be focused on the effects of inductive and capacitive coupling on high-frequency CM behavior [17]. This is due to the reason that the induced voltage drop per turn is determined by the chain flux. The complex permeability versus frequency alters the magnetic reluctance in the core, lowering the proportion of magnetizing flux and increasing the proportion of leakage flux [18]. [19] pointed out that the leakage magnetic flux significantly affects the potential distribution of primary and secondary winding, and the capacitive coupling between adjacent winding layers can also be changed. Then, the effect of leakage flux on CM transmission can be characterized by using coupling coefficients in the high-frequency model [20]. However, coupling coefficients can only be obtained by measurement and cannot be used to the prediction of EMI.

This paper addresses the emergency requirement of high frequency electromagnetic modeling of transformer, accurately predicting the nonlinear CM behaviors in a wide-band frequency range (100 kHz-100 MHz). The proposed modeling technique is developed based on the two-capacitor model. Then, a high-frequency modeling method for magnetic components that considers the effects of capacitive and inductive coupling is established. The proposed high-frequency model can be used to simulate the EMI spectrums of the whole isolated power converters. It is possible to predict whether the designed power will pass EMC certification through simulation rather than measurement.

This paper is organized as follows. In Section II, the conducted mechanism of the CM noise flowing the transformer is investigated. Then, a two-capacitance model considering only capacitive coupling and the CM behaviors evaluation method are presented. In Section III, the high-frequency CM behavior of the transformer is investigated. Combined with the nonlinear characteristics of the Mn-Zn ferrite material used as the magnetic core, a wide-band frequency CM model of the transformer is proposed. In Section IV, the parameters in the proposed model are obtained by impedance measurements and the accuracy of the proposed wide-band frequency model is checked by scattering parameter measurements. Finally, this paper is summarized.

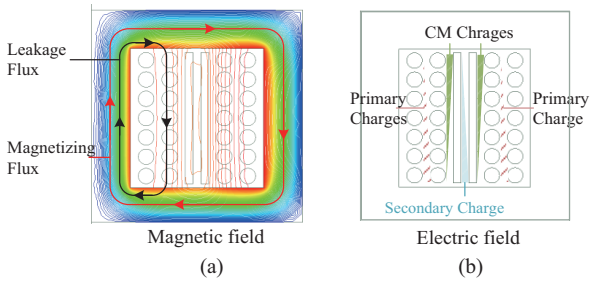

Fig. 2. Distribution of electromagnetic field. (a) Magnetic field, (b) Electric field.

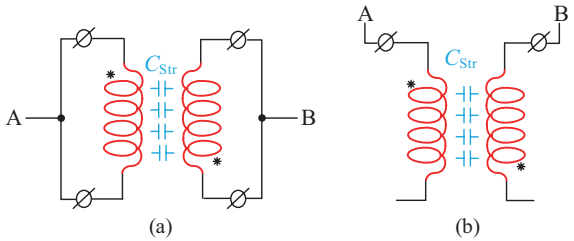

Fig. 3. Measurement method of static capacitance. (a) Method 1, (b) Method 2.

II. CM Characteristic Evaluation Method of Transformer

A. CM Transmission Mechanism

The interaction of inductive and capacitive couplings inside the core window complicates the CM noise analysis. As illustrated in Fig. 2(a), the magnetizing flux circulates only inside the magnetic core, while the leakage flux circulates through the air inside the core window. Mn-Zn ferrite material is a commonly used material in high frequency applications. Due to the characteristics of high permeability of Mn-Zn ferrite material, the proportion of leakage flux is far lower than the magnetizing flux resulting in the same induced voltage drop along each turn. Therefore, the potential distribution of the winding can be assumed to be linearly and continuous [21]. As illustrated in Fig. 2(b), there are three kinds of charges, i.e., primary charges, secondary charges and CM charges. All of them are generated by the potential difference. Primary charges and secondary charges form the primary self-capacitance and secondary self-capacitance, respectively. Only the CM charges flow through secondary side to form CM displacement current.

B. Two-capacitance Model

Since the permeability of Mn-Zn ferrite material is larger enough, the voltage potential distribution of the windings is linearly and continuedly. Then, the inductive coupling on the CM noise can be neglected, and the capacitive coupling domains the CM behaviors. Using a quantity value to represent the CM behaviors is necessary for the CM evaluation.

Fig. 3 illustrates two kinds of measurement methods of static capacitance C_{Str}, which is widely used to evaluate CM behavior. The static capacitance is measured by an LCR meter

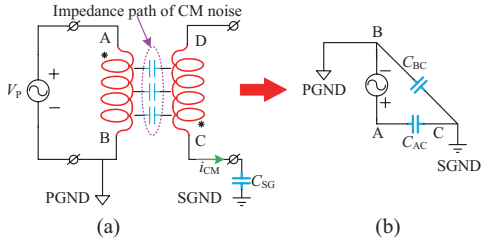

Fig. 4. Concept of dynamic CM capacitance. (a) CM transmission, (b) Two-capacitance model.

or impedance analyzer. For this kind of measurement, the two windings are regarded as a parallel plate capacitor.

The measured capacitance is determined by the winding structure parameters, such as the distance between two adjacent windings, the faced area, and the permittivity of the insulation material. Once the transformer has been wound, the value of the capacitance C_{Str} is constant and is only determined by physical structure. Hence, the measured capacitance is called static capacitance. In practical, the transformer with the same winding structure but with different winding connection type can exhibit different CM transmission characteristics. This is due to the fact that the potential distribution can affect the distribution of electric charges. Therefore, the CM transmission characteristics of a transformer is dominant by two factors, i.e., winding structure and potential distribution.

As illustrated in Fig. 4(a), an voltage excitation is assigned across the primary winding, and the electric charges is induced in the secondary winding, forming a CM displacement current i_{CM}. Fig. 4(b) illustrates the dynamic CM capacitance model containing two capacitors (C_{AD} and C_{BD}) for evaluating the CM behaviors of the transformer [9].

Assuming that the impact of leakage inductance is ignored, the potential distributions of the primary and secondary winding are shown in (1) and (2):

$$\Delta V_P = \frac{V_P}{N-1} \tag{1}$$

$$\Delta V_S = \frac{V_S}{M-1} \tag{2}$$

where N and M are the turn number of the primary and secondary windings, respectively. V_P (V_S) is the voltage drop assigned on primary winding (secondary winding) between terminal A and B (C and D).

V_{Pi} and V_{Sj} are the potential of the i turn and j turn, and they can be represented as in (3) and (4)

$$V_{Pi} = V_B + (N-i)\Delta V_P \tag{3}$$

$$V_{Sj} = V_C + (M-j)\Delta V_S \tag{4}$$

According to the displacement current rule, the CM displacement current i_{CM} flowing through the parasitic capacitance of the transformer can be calculated as following:

$$i_{CM} = \sum_{i=1}^{N}\sum_{j=1}^{M} C_{PiSj}\frac{\mathrm{d}\left(V_{Pi} - V_{Sj}\right)}{\mathrm{d}t} \tag{5}$$

where C_{PiSj} is the interwinding capacitance between i turn in primary winding and j turn in secondary winding.

Substituting (1)-(4) into (5), the CM displacement current i_{CM} can be simplified as following:

$$\begin{aligned} i_{CM} = &\sum_{i=1}^{N}\sum_{j=1}^{M} C_{PiSj}\frac{\mathrm{d}\left(V_B - V_C\right)}{\mathrm{d}t} + \\ &\sum_{i=1}^{N}\sum_{j=1}^{M} C_{PiSj}\frac{N-i}{N-1}\frac{\mathrm{d}V_P}{\mathrm{d}t} - \sum_{i=1}^{N}\sum_{j=1}^{M} C_{PiSj}\frac{M-j}{M-1}\frac{\mathrm{d}V_S}{\mathrm{d}t} \end{aligned} \tag{6}$$

Since the leakage inductance is ignored, the voltage drops V_P and V_S meets the following relationship:

$$V_P = nV_S \tag{7}$$

where n is the turn ratio of the primary to the secondary winding.

Substituting (7) into (6), the CM displacement current i_{CM} can be further simplified as:

$$\begin{aligned} i_{CM} = &\sum_{i=1}^{N}\sum_{j=1}^{M} C_{PiSj}\frac{\mathrm{d}\left(V_B - V_C\right)}{\mathrm{d}t} + \\ &\sum_{i=1}^{N}\sum_{j=1}^{M}\left(n\frac{N-i}{N-1} - \frac{M-j}{M-1}\right)C_{PiSj}\frac{\mathrm{d}V_S}{\mathrm{d}t} = \\ &C_{Str}\frac{\mathrm{d}\left(V_B - V_C\right)}{\mathrm{d}t} + C_{Str1}\frac{\mathrm{d}V_S}{\mathrm{d}t} \end{aligned} \tag{8}$$

where the coefficient C_{Str} and C_{Str1} can be expressed as:

$$C_{Str} = \sum_{i=1}^{N}\sum_{j=1}^{M} C_{PiSj} \tag{9}$$

$$C_{Str1} = n\sum_{i=1}^{N}\sum_{j=1}^{M} C_{PiSj}\frac{N-i}{N-1} - \sum_{i=1}^{N}\sum_{j=1}^{M} C_{PiSj}\frac{N-j}{M-1} \tag{10}$$

Combining the six-capacitance model from [11], the CM displacement current can be represented as:

$$\begin{aligned} i_{CM} = &\left(C_{AD} + C_{AC} + C_{BD} + C_{BC}\right)\frac{\mathrm{d}\left(V_B - V_C\right)}{\mathrm{d}t} + \\ &\left[(n-1)C_{AD} + nC_{AC} - C_{BD}\right]\frac{\mathrm{d}V_S}{\mathrm{d}t} \end{aligned} \tag{11}$$

Compared with (8) and (11), it can find that only two equations are listed in (12). Therefore, using two lumped capacitances are enough to represent the CM displacement current i_{CM}.

$$\begin{cases} C_{Str} = C_{AD} + C_{AC} + C_{BD} + C_{BC} \\ C_{Str1} = (n-1)C_{AD} + nC_{AC} - C_{BD} \end{cases} \tag{12}$$

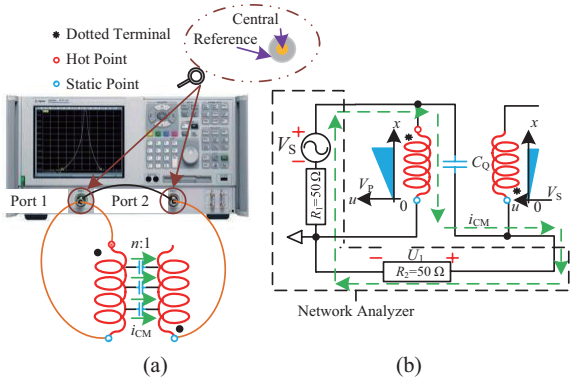

Fig. 5. Measurement method of dynamic CM capacitance of the transformer. (a) Circuit connection, (b) Equivalent circuit.

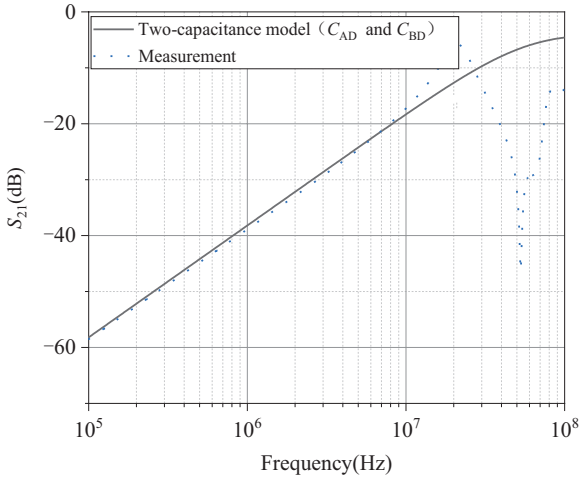

Fig. 6. Comparison between measured and the model.

C. CM Behavior Evaluation Method

To evaluate the CM transmission characteristics, Fig. 5 shows the measurement method conducted by a network analyzer. S parameter is measured for the evaluation of CM characteristics. Since the voltage excitation V_S assigned on the primary side can build the voltage potential distribution along each turn, the CM current flows through C_Q to secondary side. Then, the CM noise will be received by Port 2 of a network analyzer. For the measurement method illustrated in Fig. 5, S_{21} will be measured and used for the CM evaluation. To compare the difference between the two-capacitance model and the measurement, Fig. 6 illustrated the comparison results. It can be noticed that the two-capacitance model agrees well with the measurement from 100 kHz to 10 MHz. Besides, the slope of the two-capacitance models is 20 dB/dec up to 30 MHz. In the range of 10 MHz to 100 MHz, there is a larger discrepancy between the measurement and the two-capacitance model. The high frequency CM transmission characteristic of the transformer exhibits nonlinear behaviors. Therefore, the two-capacitance model can only represent the CM characteristics of the transformer in the frequency range from 100 kHz to 10 MHz. In this frequency range, only the capacitive coupling between adjacent primary and secondary winding layers is considered. For higher frequency range, only considering the capacitive coupling is insufficient to model the high frequency CM characteristics. It is necessary to consider both the effect of inductive coupling and capacitive coupling on the high frequency CM behavior.

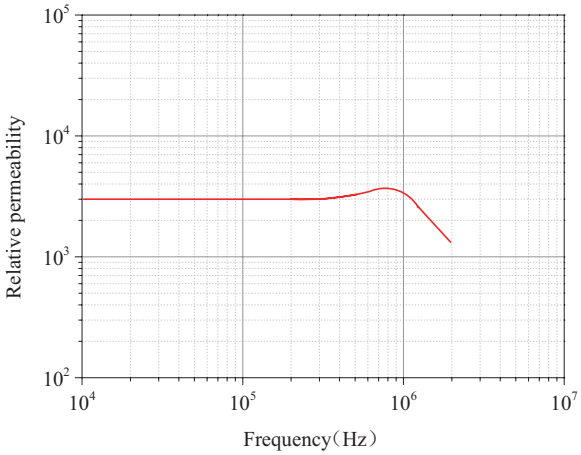

Fig. 7. Relative permeability of the PC95 core material.

As has been analyzed in Fig. 2, both high-frequency electric field and high-frequency magnetic field exist in the core window of the transformer. Since Mn-Zn ferrite material is used as the magnetic core, the permeability changes rapidly with frequency after the cut-off frequency [17]. Fig. 7 illustrated the curve of the relative permeability versus frequency of the Mn-Zn ferrite material. This kind of Mn-Zn ferrite material is called PC95, which is manufactured by TDK. Once the frequency is higher than the cut-off frequency of the magnetic material (For Mn-Zn ferrite, its cut-off frequency is 1 MHz), the permeability will rapidly decrease, resulting in a large proportion variation between the leakage flux and the magnetizing flux. Since the flux linkage each turn is different, the voltage potential distribution along each turn cannot be regarded as linear and continuous. Hence, the effect of the inductive coupling should be further considered in modeling high-frequency CM behavior. For coupled hollow inductors, they do not have a magnetic core as a coupling medium. In the high frequency range, The CM transmission characteristics is not affected by the nonlinear characteristics of the magnetic core. The CM transmission characteristics between primary and secondary winding only take into account the effect of electric field coupling, and can be represented in terms of capacitance.

III. Modeling of High Frequency Transformers

As has been analyzed in Section II, the magnetic characteristics of permeability with frequency are the main factor contributing to the nonlinear CM behavior in the high-frequency range. In order to characterize the CM transmission behavior, it is crucial to accurately measure the complex permeability of magnetic material. However, many manufactures only provide information on the variation of amplitude permeability with frequency (lack of phase information) and a limited frequency

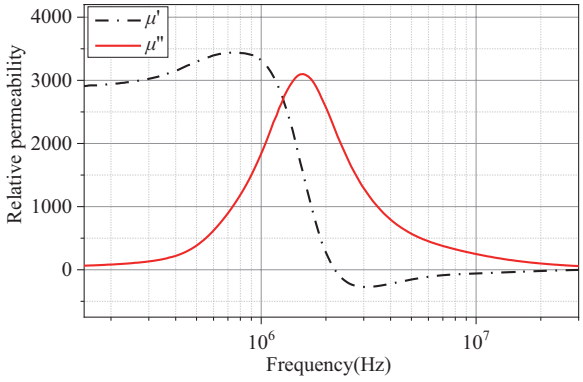

Fig. 8. Complex relative permeability versus frequency.

range (10 kHz-2 MHz), as illustrated in Fig. 7. It is insufficient for modeling and analysis of EMI in a wide-band frequency range for EMI modeling.

A. Measurement of Magnetic Characteristics

In this paper, complex permeability is introduced, which can be used to analyze the high-frequency CM conduction mechanism.

$$\mu = \mu' - j\mu'' \tag{13}$$

where μ' is the real part reflecting the magnetizing characteristic of the magnetic material, and μ'' is the imaginary part reflecting the loss characteristics.

In order to achieve a wide-band EMI modeling of the transformer, it is essential to measure the complex permeability of the magnetic material. In this paper, PC95 Mn-Zn ferrite manufactured by TDK was used, which Fig. 8 shows the measurement results of complex permeability versus frequency.

It can be clearly observed that both μ' and μ'' vary with frequency. For the real part μ', the cut-off frequency is 1 MHz, and after the cut-off frequency, the real part rapidly decreases leading to a decrease in the magnetizing flux and an increase in the leakage flux.

B. Proposed High Frequency Model

Since the electric field distribution inside the transformer varies with frequency, capacitive coupling is affected by inductive coupling in the higher frequency range.

For two-capacitance model, the branches of leakage inductance and magnetizing inductance are regarded as short-circuit and open-circuit, respectively. This model should follow two assumptions:

1. The permeability of the core material is higher enough.
2. The magnetizing inductance is far larger than the leakage inductance.

As illustrated in Fig. 9(a), the transformer is regarded as an ideal transformer which propagates the CM noise through the two capacitances (C_{AC} and C_{BC}). However, as illustrated in Fig. 8, the permeability of the magnetic core varies with frequency. When the frequency is higher than the cut-off frequency (1

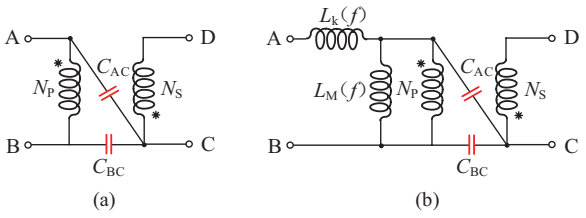

Fig. 9. High frequency model of transformer. (a) Two-capacitance model, (b) Proposed model.

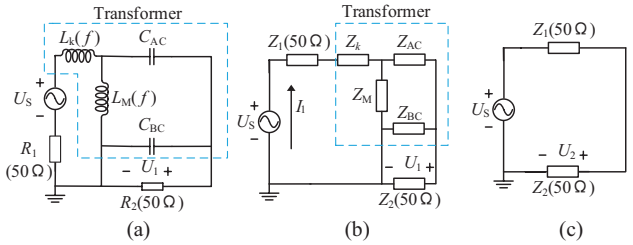

Fig. 10. Equivalent circuit model. (a) Equivalent circuit with transformer, (b) Equivalent circuit with transformer in form of impedance, (c) Equivalent circuit without transformer.

MHz), the two assumptions are not valid. As shown in Fig. 6, the measured S_{21} parameter exhibits nonlinear characteristics within the range of 10 MHz to 100 MHz. Since the permeability decreases rapidly after the cut-off frequency, there is a significant discrepancy between the two-capacitance model and the S_{21} measurement results. The proposed model should consider the impacts of leakage inductance and magnetizing inductance on conducted EMI. As illustrated in Fig. 9(b), the developed high-frequency model further takes into account the effects of leakage inductance and magnetizing inductance with frequency.

Fig. 10(a) illustrates the equivalent circuit of the proposed high frequency transformer model under the measured configuration of S_{21} parameter. For better and clear modeling, the branch impedance of $L_k(f)$ and $L_M(f)$ can be represented in form of the impedance Z_k and Z_M, respectively, as shown in Fig. 10(b).

According to the definition of S_{21} parameter, it can be given as:

$$S_{21}(\text{dB}) = 20\lg\left|\frac{U_1}{U_2}\right| \tag{14}$$

where U_1 is the voltage drop in resistor R_2 with a transformer as shown in Fig. 10(b) and U_2 is the voltage drop in resistor R_2 without transformer as shown in Fig. 10(c).

The total displacement current I_1 is given as:

$$I_1 = \frac{U_S}{Z_k + Z_1 + Z_M // \left(Z_{AC} + Z_2 // Z_{BC}\right)} \tag{15}$$

The voltage drops U_1 and U_2 across the impedance Z_2 in both cases can be derived as:

$$U_1 = I_1 \frac{Z_M}{Z_M + \left(Z_{AC} + Z_2 // Z_{BC}\right)} \left(Z_2 // Z_{BC}\right) \tag{16}$$

$$U_2 = \frac{50}{100} \cdot U_S \tag{17}$$

By substituting (16) and (17) into (14), the S_{21} parameter can be represented as:

$$S_{21}(\text{dB}) = 20\lg\left(\left|\frac{2}{Z_k + Z_1 + Z_M // \left(Z_{AC} + Z_2 // Z_{BC}\right)} \cdot \frac{Z_M\left(Z_2 // Z_{BC}\right)}{Z_M + \left(Z_{AC} + Z_2 // Z_{BC}\right)}\right|\right) \tag{18}$$

From (18), it can find that when the magnetizing impedance Z_M is larger enough, the impact of leakage impedance Z_k can be neglected. For the two-capacitance model, the leakage impedance Z_k is regarded as short-circuit and the magnetizing impedance is regarded as open-circuit.

Similarly, when the two-capacitance model is applied, the S_{21} parameter can be given as:

$$S_{21}(\text{dB}) = 20\lg\left(\left|\frac{2Z_2}{Z_1 + Z_2 + Z_{AC}}\right|\right) \tag{19}$$

As the frequency increases, the permeability decreases rapidly, resulting in significant changes in both Z_k and Z_M. When the frequency is above the cut-off frequency of the magnetic material, the impedance Z_k and Z_M exhibit nonlinear characteristics. For this consideration, the leakage impedance and magnetizing impedance should be considered in the high frequency range. Therefore, the proposed high frequency model can consider both the effect of capacitive and inductive couplings on conducted EMI.

IV. Extraction of Parameters for the Proposed Model

For the proposed high-frequency model, it includes capacitive parameters and inductive parameters, which need to be obtained through measurements.

A. Capacitive Parameters

The capacitive parameters include the lumped capacitance C_{AC} and C_{BC}, which are determined by the structure capacitance C_{Str} defined in (9) and the voltage difference (U_{AC} and U_{BC}) between two terminals (A and C, B and C). The structure capacitance C_{Str} is measured by an impedance analyzer as shown in Fig. 11(a). Then, the voltage pulsation generated by the signal generator is applied to the primary winding. As show in Fig. 11(b) and (c), U_{AC} and U_{BC} are measured by voltage probes using an oscilloscope. It should be noticed that the influence of the probe's parasitic capacitance on the measurement results should be considered during the measurement.

As shown in Fig. 11(b), for this configuration, the voltage drops U_{AB} and U_{AC} satisfy the following relationship:

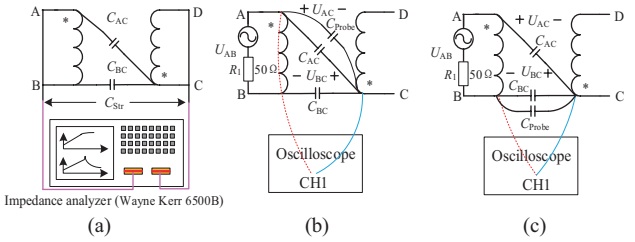

Fig. 11. Extraction method of capacitive parameters. (a) Measurement of structure parameter, (b) Measurement of C_{BC}, (c) Measurement of C_{AC}.

$$\frac{U_{AC}}{U_{AB}} = \frac{\dfrac{1}{\text{j}\omega(C_{AC} + C_{Probe})}}{\dfrac{1}{\text{j}\omega(C_{AC} + C_{Probe})} + \dfrac{1}{\text{j}\omega C_{BC}}} = \frac{C_{BC}}{C_{AC} + C_{BC} + C_{Probe}} = \frac{C_{BC}}{C_{Str} + C_{Probe}} \tag{20}$$

where U_{AB} is the voltage drop determined by a signal generator, and U_{AC} is the measured voltage drop.

It should be noticed that the value of C_{AC}, C_{BC} and C_{Probe} are in pF level resulting in Z_{AC}, Z_{BC}, Z_{Probe},>>50 Ω. Therefore, the resistor R_1 (50 Ω) can be omitted in the calculation.

According to (20), C_{BC} can be transformed as:

$$C_{BC} = \left(C_{Str} + C_{Probe}\right)\frac{U_{AC}}{U_{AB}} \tag{21}$$

Similarly, as shown in Fig. 11(c), when the voltage drop U_{BC} is measured, the voltage drops U_{AB} and U_{BC} satisfy the following relationship:

$$\frac{U_{BC}}{U_{AB}} = \frac{\dfrac{1}{\text{j}\omega(C_{BC} + C_{Probe})}}{\dfrac{1}{\text{j}\omega(C_{BC} + C_{Probe})} + \dfrac{1}{\text{j}\omega C_{AC}}} = \frac{C_{AC}}{C_{AC} + C_{BC} + C_{Probe}} = \frac{C_{AC}}{C_{Str} + C_{Probe}} \tag{22}$$

According to (22), C_{AC} can be transformed as:

$$C_{AC} = \left(C_{Str} + C_{Probe}\right)\frac{U_{BC}}{U_{AB}} \tag{23}$$

Based on the derivation (20)-(23), the capacitance C_{BC} and C_{AC} can be given as following:

$$\begin{cases} C_{BC} = \left(C_{Str} + C_{Probe}\right)\dfrac{U_{AC}}{U_{AB}} \\ C_{AC} = \left(C_{Str} + C_{Probe}\right)\dfrac{U_{BC}}{U_{AB}} \end{cases} \tag{24}$$

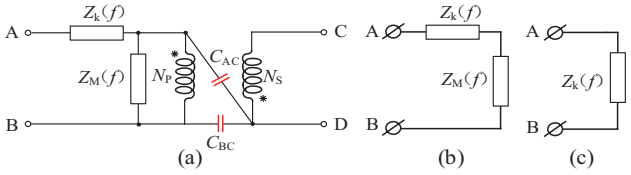

Fig. 12. Transformer model. (a) Proposed high frequency model, (b) Open-circuit operation, (c) Short-circuit operation.

Besides, the C_{AC} and C_{BC} also satisfy the following relationship:

$$C_{Str} = C_{AC} + C_{BC} \tag{25}$$

B. Inductive Parameters

The inductive parameters in the proposed model include the leakage impedance and the magnetizing impedance, both of which can be afforded by impedance measurements.

Fig. 12(a) illustrated the proposed high-frequency model. For extracting the magnetizing impedance Z_M, the secondary side should be opened and the corresponding circuit is shown in Fig. 12(b). For this operation, the measured impedance between terminals A and B includes the sum of the magnetizing impedance and the leakage impedance. Since the magnetizing impedance Z_M is far larger than the leakage impedance Z_k, the measured impedance is almost equal to the magnetizing impedance Z_M.

Similarly, the leakage impedance can be obtained by a short-circuit operation on the secondary side, the corresponding equivalent circuit of which is illustrated in Fig. 12(c). When the secondary side is short-circuited, the magnetizing flux within the magnetic core is zero. Therefore, the measured impedance contains only the leakage impedance without the magnetizing inductance. For the measured impedance $Z_M(f)$ and $Z_k(f)$, they will be substituted into the model as shown in Fig. 12.

V. Experiment Verification

For verifying the effectiveness of the proposed high frequency model of the transformer, a wire-wound transformer is made and used to measure the CM transmission characteristics. Fig. 13(a) shows prototype of the test transformer and Fig. 13(b) illustrates its winding arrangement. The detail specifications of the transformer are listed in Table I. The core material is PC95 and its permeability versus frequency is illustrated in Fig. 8.

In order to measure the S_{21} parameter, a network analyzer can be used. In the measurements, an Agilent E5072A network analyzer was applied to measure the CM transmission characteristics of the transformer (S_{21} versus frequency in the range of 100 kHz to 100 MHz). Fig. 14 illustrated the measurement platform of S_{21} parameter.

It should be noticed that calibration is necessary to achieve high accuracy measurements in the high frequency range. Therefore, the SOLT (Short-Open-Load-Through) calibration method is used to ensure the accuracy of radio frequency (RF) measurements. In order to meet the impedance matching, the transmission board used to measure S_{21} should be designed

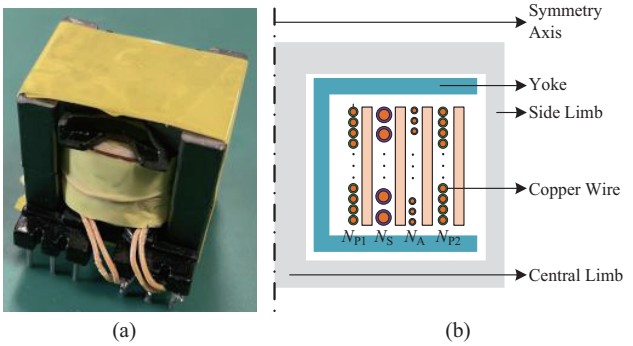

Fig. 13. Prototype of the test transformer. (a) Prototype, (b) Winding arrangement.

TABLE I
Specifications of the Transformer

Parameters	Value
Core size	PQ2625
Core material	PC95 (Manufactured by TDK)
Initial relative permeability	3300
Bobbin	6+6 YT-2606
Winding diameter	d_P=0.4mm; d_S=0.6 mm (bifilar winding); d_A=0.3 mm
Winding arrangement	PSP N_{P1}=17, N_{P2}=17; N_A=6; N_S=8

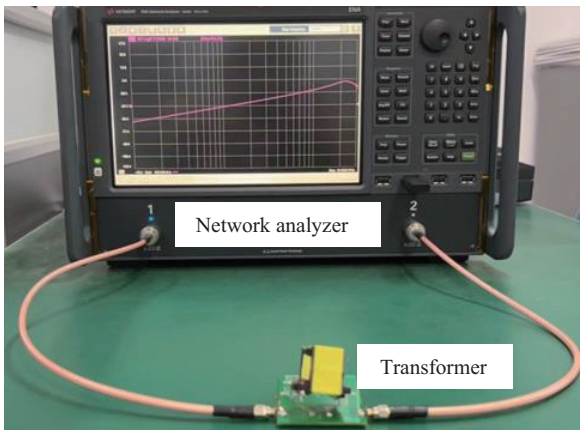

Fig. 14. Measured platform of S_{21} parameter.

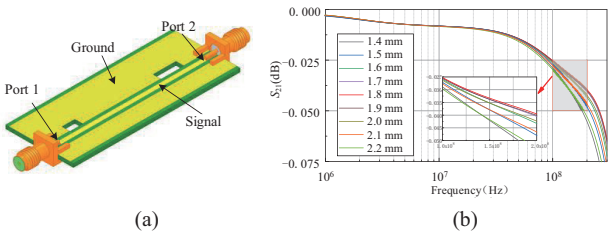

Fig. 15. Design of high-frequency test board. (a) Test board, (b) Influence of signal cable widths on S_{21} measurement.

for 50 Ω, as shown in Fig. 15(a). If the impedance matching is done properly, the signal from Port 1 will be completely re-

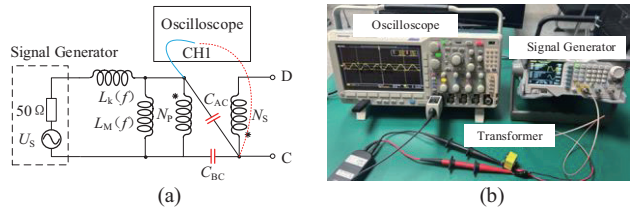

Fig. 16. Extraction of capacitive parameters C_{AC} and C_{BC}. (a) Connection schematic, (b) Extraction platform.

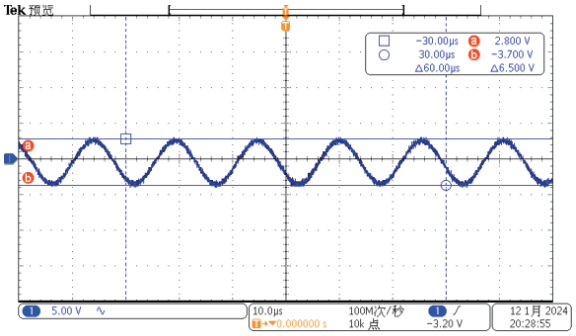

Fig. 17. Measurement of voltage waveform of U_{AC}.

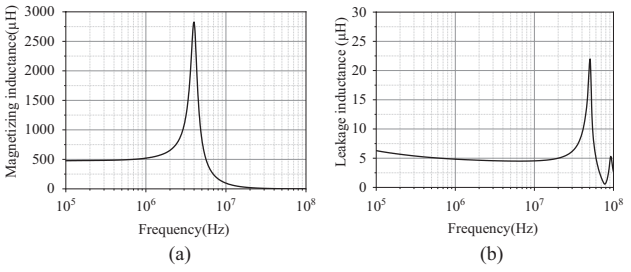

Fig. 18. Measured impedance. (a) Magnetizing inductance, (b) Leakage inductance.

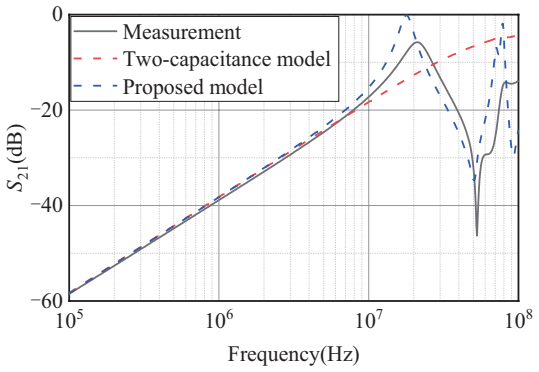

Fig. 19. Comparison results.

ceived by Port 2. Since there are some differences between the transmission calibration board and the microstrip line, the characteristics impedance of the test board is designed to 50 Ω. To be more precise, the FEM simulation tool is used to fine-tune the line width of the signal line to achieve better measurements. Fig. 15(b) shows the simulation results of the transmission coefficient S_{21} for different signal wire width, from which a suitable line width size of 1.8 mm was selected. The transmission coefficient is related to the characteristic impedance of the line; The closer the transmission coefficient is to 1 (S_{21} is close to 0 dB), the closer the characteristic impedance is to 50 Ω.

Fig. 16(a) shows the measurement diagram of the capacitive parameters, i.e., C_{AC} and C_{BC}, where a signal generator and an oscilloscope is used. The signal generator generates high-frequency voltage pulsations U_S on the primary winding and the CM noise will flow through the lumped capacitance C_{AC} and C_{BC} to secondary side. Fig. 16(b) shows the capacitance extraction platform where the oscilloscope is a Tek MDO3014 and the signal generator is a RIGOL DG1062Z. As has been mentioned in Section IV, the impact of probe capacitance should be taken into account when measuring parasitic capacitance. The voltage probe (Tek THDP0200) has a parasitic capacitance C_{Probe} of 15 pF according to the data sheet provided by Tektronix. The structure capacitance C_{Str} is 44.85 pF, where the used impedance analyzer is WK6500B. The amplitude of the sinusoidal signal U_S is 20 V and the frequency is 50 kHz. The lumped capacitance C_{BC} and C_{AC} are selected, and the lumped capacitance C_{AD} and C_{BD} are set to 0. Fig. 17 shows the measured voltage waveform of U_{AC}, and its amplitude is 6.5 V.

Based on the measured waveform shown in Fig. 17 and the relationship between the voltages and the parasitic capacitances in (21), the lumped capacitance C_{BC} and C_{AC} can be calculated by (24) and (25). Therefore, the lumped capacitance C_{BC} and C_{AC} are 19.451 pF and 25.399 pF, respectively.

Fig. 18(a) shows the measured magnetizing inductance of the transformer. The magnetizing inductance remains almost the same in the frequency range from 100 kHz to 500 kHz with a resonance point occurring at 4 MHz. When the frequency is higher than 4 MHz, the magnetizing inductance will decrease rapidly. This phenomenon is because that the inherent high-frequency magnetic characteristics of the core material.

Fig. 18(b) shows the measured leakage inductance versus frequency. Similarly, the resonance point occurs at 50 MHz. The reason why the resonance point of the leakage inductance curve is far higher than that of the magnetizing inductance curve is due to the reason that the leakage flux flows through the air instead of the core material. The relative permeability of the air is equal to 1, and does not vary with frequency. Then, the resonance frequency due to leakage inductance and parasitic capacitance is far higher than that due to magnetizing inductance and parasitic capacitance. The measured L_k and L_M versus frequency shown in Fig. 18, will be substituted into (18). Combining with the measured C_{AC} and C_{BC}, the S_{21} parameter versus frequency will be calculated.

For full-circuit EMI prediction, it requires the models of PCB traces, rectifier bridge, near field couplings, magnetic components, and EMI receivers. All of the models will affect the EMI simulation accuracy. Besides, the EMI modeling process of the full-circuit needs to extract the numerous of parameters used in EMI prediction. Limited by the page length, the validation of the proposed model is focused on single transformer evaluation. Based on the extracted parameters, Fig. 19 illustrates the comparison results between the S_{21} measurements, the two-capacitor model and the proposed high-fre-

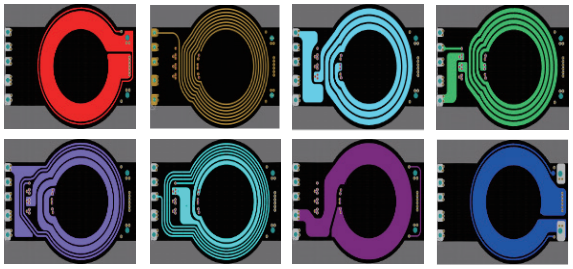

Fig. 20. Winding arrangement of a PCB planar transformer.

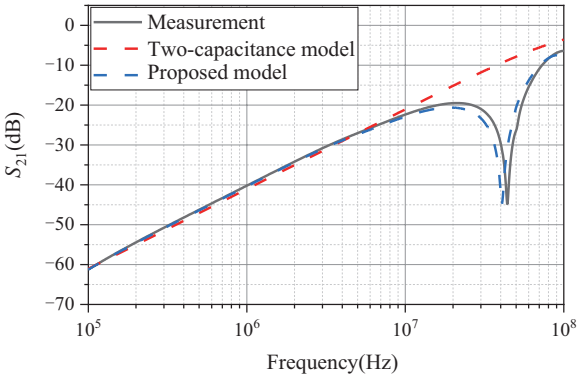

Fig. 21. Comparison results of a PCB planar transformer.

quency model. It can be vividly observed that the two-capacitor model exhibits linear and continued characteristics in all frequency range (100 kHz-100 MHz). As analyzed in Section III, the two-capacitance model can represent the CM transmission characteristics from 100 kHz to 10 MHz. This is because that the two-capacitance model does not take into account the effect of inductive coupling on CM transmission, resulting in a slope equal to 20 dB/dec. The proposed model agrees well with the measurements in all frequency ranges. Since it can fulfill take into account the effect of both capacitive and inductive coupling, the proposed high-frequency model can exhibit almost the same CM transmission characteristics as the measured results in the range of 100 kHz to 100 MHz.

The proposed high-frequency transformer model can be applied in both wire-wound transformers and PCB planar transformers. In order to illustrate the generalization of the proposed high-frequency modeling method, the PCB planar transformer will be taken as an example. The detail PCB winding specifications are shown in Fig. 20. Fig 21 illustrated the corresponding comparison results, where the proposed model can agree well with the measurement in the frequency range from 100 kHz to 100 MHz.

In order to illustrate the effect of leakage flux on CM noise transmission, Fig. 22 shows the CM noise transmission characteristics under different leakage inductance L_k. It can be vividly found that the larger the leakage inductance L_k, the smaller the resonance frequency of the CM transmission characteristics line. Therefore, the value of leakage inductance will significantly affect the high-frequency CM transmission characteristics of the transformer. The modeling process is the same whether the leakage flux is large or small.

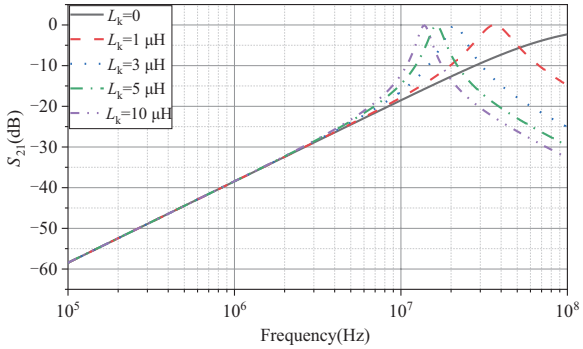

Fig. 22. Effect on leakage inductance on CM transmission.

In summary, inductive coupling can significantly affect the capacitive CM transmission characteristics, and lead to nonlinear CM transmission in the high-frequency range.

VI. Conclusion

Inductive and capacitive parasitic parameters can significantly affect the CM noise transmission characteristics. Existing techniques for modeling transformer CM behavior only consider the influence of electric field coupling on CM transmission and have a limited frequency range (below 10 MHz) for EMI prediction. The frequency-dependent characteristic of the permeability leads to nonlinear CM transmission characteristics in the high-frequency range. The proposed high-frequency model further takes into account the effects of magnetic and electric field on CM transmission, and can accurately represent CM transmission in a wide-band frequency range (100 kHz to 100 MHz). The proposed high-frequency model can be further developed and used for the EMI prediction of the whole circuit. However, the proposed high-frequency model has not yet been used to investigate the radiated EMI emission mechanism and can be developed in future work.

References

[1] J. Yao, S. Wang, and Z. Luo, "Modeling, analysis, and reduction of radiated EMI due to the voltage across input and output cables in an automotive non-isolated power converter," in *IEEE Transactions on Power Electronics*, vol. 37, no. 5, pp. 5455–5465, May 2022.

[2] F. C. Lee, Q. Li, Z. Liu, Y. Yang, C. Fei, and M. Mu, "Application of GaN devices for 1 kW server power supply with integrated magnetics," in *CPSS Transactions on Power Electronics and Applications*, vol. 1, no. 1, pp. 3–12, Dec. 2016.

[3] X. Jia, C. Hu, B. Dong, F. He, H. Wang, and D. Xu, "Influence of system layout on CM EMI noise of SiC electric vehicle powertrains," in *CPSS Transactions on Power Electronics and Applications*, vol. 6, no. 4, pp. 298–309, Dec. 2021.

[4] Z. Huang, G. Son, Q. Li, and F. C. Lee, "Balance techniques and PCB winding magnetics for common-mode EMI noise reduction in three-phase AC-DC converters," in *IEEE Transactions on Power Electronics*, vol. 37, no. 3, pp. 3130–3142, Mar. 2022.

[5] H. -P. Park, M. Kim, and J. -H. Jung, "Spread spectrum technique to reduce EMI emission for an LLC resonant converter using a hybrid modulation method," in *IEEE Transactions on Power Electronics*, vol. 33, no. 5, pp. 3717–3721, May 2018.

[6] M. Antivachis, P. S. Niklaus, D. Bortis, and J. W. Kolar, "Input/output EMI filter design for three-phase ultra-high speed motor drive gan inverter stage," in *CPSS Transactions on Power Electronics and Applications*,

vol. 6, no. 1, pp. 74–92, Mar. 2021.
[7] H. Chen, C. Zhao, and Z. Zheng, "Design of the number of transformer shielding winding turns for minimizing low-frequency common-mode noise in flyback converters," in *IEEE Transactions on Electromagnetic Compatibility*, vol. 61, no. 6, pp. 1961–1966, Dec. 2019.
[8] H. Chen and G. Liu, "Determination of the width of shielding foil in sandwiched winding transformer for minimizing common mode EMI of flyback converters," in *IEEE Transactions on Electromagnetic Compatibility*, vol. 62, no. 2, pp. 639–642, Apr. 2020.
[9] Y. Li, H. Zhang, S. Wang, H. Sheng, C. P. Chng, and S. Lakshmikanthan, "Investigating switching transformers for common mode EMI reduction to remove common mode EMI filters and Y-capacitors in flyback converters," in *IEEE Journal of Emerging and Selected Topics in Power Electronics*, vol. 6, no. 4, pp. 2287–2301, Dec. 2018.
[10] Y. Li, H. Zhang, S. Wang, H. Sheng, S. Lakshmikanthan, and C. P. Chng, "Techniques of the modeling, measurement and reduction of common mode noise for a multi-winding switching transformer," in *2017 IEEE Applied Power Electronics Conference and Exposition (APEC)*, Tampa, FL, USA, 2017, pp. 2511–2518.
[11] T. Duerbaum, "Capacitance model for magnetic devices," in *2000 IEEE 31st Annual Power Electronics Specialists Conference. Conference Proceedings (Cat. No.00CH37018)*, Galway, Ireland, 2000, pp. 1651–1656.
[12] H. Zhang, S. Wang, Y. Li, Q. Wang, and D. Fu, "Two-capacitor transformer winding capacitance models for common-mode EMI noise analysis in isolated DC–DC converters," in *IEEE Transactions on Power Electronics*, vol. 32, no. 11, pp. 8458–8469, Nov. 2017.
[13] H. Chen, Z. Zheng, and J. Xiao, "Determining the number of transformer shielding winding turns for suppressing common-mode noise in flyback converters," in *IEEE Transactions on Electromagnetic Compatibility*, vol. 60, no. 5, pp. 1606–1609, Oct. 2018.
[14] K. Fu and W. Chen, "Evaluation method of flyback converter behaviors on common-mode noise," in *IEEE Access*, vol. 7, pp. 28019–28030, 2019.
[15] L. Xie, X. Ruan, and Z. Ye, "Equivalent noise source: an effective method for analyzing common-mode noise in isolated power converters," in *IEEE Transactions on Industrial Electronics*, vol. 63, no. 5, pp. 2913–2924, May 2016.
[16] L. Xie, X. Ruan, H. Zhu, and Y. -K. Lo, "Hybrid passive cancelation method for reducing common-mode noise in isolated power converters," in *IEEE Transactions on Power Electronics*, vol. 36, no. 1, pp. 391–400, Jan. 2021.
[17] K. Fu, L. Dai, and W. Lan, "Modeling and analysis of CM noise behaviors of transformers in power converters," in *Journal of Electrical Engineering & Technology*, vol. 19, no.1, pp. 297–310, Apr. 2023.
[18] M. Kącki, M. S. Ryłko, J. G. Hayes, and C. R. Sullivan, "Measurement methods for high-frequency characterizations of permeability, permittivity, and core loss of Mn-Zn ferrite cores," in *IEEE Transactions on Power Electronics*, vol. 37, no. 12, pp. 15152–15162, Dec. 2022.
[19] J. Dong, X. Chen, and S. Lin, "Electro-magnetic interference model of transformer considering the leakage magnetic field," in *Transactions of China Electrotechnical Society*, vol. 32, no.21, pp. 143–152, Nov. 2017.
[20] S. Lin, W. Chen, J. Dong, and Q. Chen, "Magneto-electric composite model of transformer for conducted common-mode EMI in switching-mode power supply," in *Proceedings of the Chinese Society of Electrical Engineering*, vol. 37, no. 8, pp. 2436–2445, Apr. 2017.
[21] K. Fu and W. Chen, "Balance winding scheme to reduce common-mode noise in flyback transformers," in *Journal of Power Electronics*, vol. 19, no. 1, pp. 296–306, Jan. 2019.

Kaining Fu was born in Xiamen, China, in 1993. He received his M.S. and Ph.D. degrees from Fuzhou University, Fuzhou, China, in 2018 and 2021, respectively. He is presently working as a lecturer in the College of Electrical Engineering and Automation, Xiamen University of Technology, Xiamen, China. He is a member of the Magnetic Technology Committee of the China Power Supply Society (CPSS). His current research interests include power conversion, high-frequency magnetics, EMI debugging and solutions, and electromagnetic field analysis and applications.

Jiangtao Tu was born in Datian, Fujian, in 2001. He is presently working towards his M.S. degree in the College of Electrical Engineering and Automation, Xiamen University of Technology, Xiamen, China. His current research interest includes electromagnetic interference in power converters.

Wei Chen was born in Fuzhou, China. He received his M.S. and Ph.D. degrees from Fuzhou University, Fuzhou, China, in 1987 and 1990, respectively. He worked as a senior visiting professor in the Center for Power Electronics Systems (CPES), Virginia Tech, Blacksburg, Virginia, USA, from 1996 to 1998. He was with Delta Electronics Co., Ltd., as a R&D manager in the Delta Power Electronics Center, Shanghai, China, from 1999 to 2008. He has published more than 80 technical papers, including IEEE transactions and proceedings. He has held more than 40 approved patents in China and the USA. His current research interests include power conversion, high-frequency magnetic technology, EMI debugging and solutions, wireless power transfer, and electromagnetic field analysis and its applications. Professor Chen is an executive member of the council of the China Power Supply Society (CPSS) and he served as chairman of the Magnetic Component Specialty Committee of the CPSS.

Linsen Huang received the B.Sc. degree from the Minnan Normal University, Zhangzhou, China, in 2013, the M.Sc. degree from the Hunan University of Technology, Zhuzhou, China, in 2015, and the Ph.D. degree from Jiangsu University, Zhenjiang, China, in 2022, all in electrical engineering. He has been with Xiamen University of Technology since 2023, where he is currently a Lecturer in the School of Electrical Engineering and Automation. His research interests include electrical machine control and power electronic converters.